AIP | Review of Scientific Instruments

Development of ion beam figuring system with electrostatic deflection for ultraprecise X-ray reflective optics

Jumpei Yamada, Satoshi Matsuyama, Yasuhisa Sano, and Kazuto Yamauchi

Citation: Review of Scientific Instruments **86**, 093103 (2015); doi: 10.1063/1.4929323
View online: http://dx.doi.org/10.1063/1.4929323
View Table of Contents: http://scitation.aip.org/content/aip/journal/rsi/86/9?ver=pdfcov
Published by the AIP Publishing

Development of ion beam figuring system with electrostatic deflection for ultraprecise X-ray reflective optics

Jumpei Yamada, Satoshi Matsuyama,[a] Yasuhisa Sano, and Kazuto Yamauchi
Department of Precision Science and Technology, Graduate School of Engineering, Osaka University, 2-1 Yamada-oka, Suita, Osaka 565-0871, Japan

(Received 29 May 2015; accepted 7 August 2015; published online 1 September 2015)

We developed an ion beam figuring system that utilizes electrostatic deflection. The system can produce an arbitrary shape by deterministically scanning the ion beam. The scan of the ion beam, which can be precisely controlled using only an electrical signal, enables us to avoid degradation of the mirror shape caused by imperfect acceleration or deceleration of a mechanically scanning stage. Additionally, this surface figuring method can easily be combined with X-ray metrology because the workpiece remains fixed during the figuring. We evaluated the figuring accuracy of the system by fabricating a plano-elliptical mirror for X-ray focusing. A mirror with a shape error of 1.4 nm root mean square (RMS) with a maximum removal depth of 992 nm, which corresponds to figuring accuracy of 0.14% RMS, was achieved. After the second shape corrections, an elliptical shape with a shape error of approximately 1 nm peak-to-valley, 0.48 nm RMS could be fabricated. Then, the mirror surface was smoothed by a low-energy ion beam. Consequently, a micro-roughness of 0.117 nm RMS, measured by atomic force microscopy, was achieved over an area of 1×1 μm^2. © *2015 AIP Publishing LLC.* [http://dx.doi.org/10.1063/1.4929323]

I. INTRODUCTION

In third-generation synchrotron radiation facilities and X-ray free-electron laser facilities, it is essential to focus X-rays in order to perform high-sensitivity and high-resolution analysis. X-ray mirrors are used widely to produce nanofocused X-ray beams[1] owing to their high throughput, large acceptable aperture, and achromaticity. However, X-ray mirrors require a shape accuracy of a few nanometers to realize diffraction-limited focusing because X-ray wavelengths are so short that only such high-quality mirrors can satisfy Rayleigh's quarter-wavelength rule.[2] Additionally, the surface roughness should be equivalent to that of a high-quality silicon wafer, in order not to degrade the reflectivity.[3] To realize ultraprecise X-ray mirrors, various surface figuring techniques such as elastic emission machining (EEM),[4,5] plasma chemical vaporization machining (PCVM),[6,7] magnetorheological finishing (MRF),[8] and computer-controlled polishing (CCP)[9] have been developed. Moreover, optical metrology such as stitching interferometers (micro stitching interferometer (MSI), relative angle determinable stitching interferometer (RADSI))[10,11] and slope profilers (long trace profiler (LTP), nanometer optical component measuring machine (NOM))[12,13] have been developed to measure aspherical shapes with an accuracy of a few nanometers. However, we think that mirror fabrication techniques need further improvements to overcome the following problems: (a) influence by wet processing, (b) imperfect feed speed introduced by a mechanically scanning stage, and (c) poor measurement accuracy for mirrors with large numerical aperture. With respect to (a), wet processing techniques are not suitable for complex mirrors such as bimorph mirrors,[14] which are assembled with glue. With respect to (b), conventional computer-controlled machining suffers from imperfect feed speed, which results in figure errors on mirrors, because the scanning velocity of the worktable or processing tool is controlled using mechanical stages.[15] Problem (c) arises because current measurement systems have difficulty in measuring mirrors with a steeply curved shape with high accuracy,[16] although they can precisely measure nearly planar shapes.

Ion beam figuring (IBF) has been used for the fabrication of high-performance optics owing to its characteristics such as non-contact and dry processing, highly deterministic figuring, lower surface damage, and material removal efficiency.[17,18] The other attractive feature of ion beams is that deflection of ions can easily be accomplished with significantly high accuracy. Electrostatic deflection enables us to precisely scan an ion beam instead of mechanically scanning stage, which eliminates imperfections in the scanning velocity. Moreover, surface figuring by scanning the ion beam can be combined easily with X-ray metrology[19] because the workpiece can remain completely fixed during the figuring. X-ray metrology has attracted much attention because it can measure steeply curved shapes with high accuracy and measure X-ray mirrors under practical usage settings.[16,20] Additionally, low-energy ion beams can smooth the material surface.[21] This is highly desirable for the fabrication of X-ray mirrors that require atomically smooth surfaces to obtain high reflectivity.

We developed an ion beam figuring system that utilizes electrostatic deflection, which consists of an ion beam gun and a deflection system. The system can produce an arbitrary shape on a substrate by deterministically controlling the electric field intensity and can also smooth the mirror surface with a low-energy ion beam without changing the system. In this paper, we describe the development of the IBF system and

[a]Author to whom correspondence should be addressed. Electronic mail: matsuyama@prec.eng.osaka-u.ac.jp

fabrication of an elliptical focusing mirror for hard X-rays. The figuring accuracy of the system was evaluated by measuring the fabricated shape. Moreover, the surface roughness just after processing and after the smoothing was investigated in detail.

II. ION BEAM FIGURING SYSTEM WITH ELECTROSTATIC DEFLECTION

A. Ion beam gun

Inductively coupled plasma (ICP) source was employed in the ion beam gun. Fig. 1 shows a schematic of the ion beam gun. Ions are extracted from Ar plasma generated by a radio frequency (RF) power supply of 13.56 MHz. Then, ions are accelerated in a range from 1.0 to 5.0 kV and focused down to a full width at half maximum (FWHM) of 0.6-1.6 mm by three-stage einzel lenses. The vacuum chamber and inside of the ion beam gun can reach a base pressure of 10^{-6} Pa. A removal rate of 8.32×10^{-3} mm^3/h for Si(001) is obtainable in our ion beam gun. Table I lists the specifications of the ion beam gun.

B. Ion beam deflection system

In order to realize highly accurate computer-controlled figuring, we developed a beam deflection system using an electric field produced by parallel-plate electrodes, as shown in Fig. 2. Because the displacement of an ion beam at the sample plane is precisely proportional to the change of the electric field, the electrostatic deflection is very suitable for controlling the ion beam trajectory. When an ion beam with an accelerating voltage of V_0 is deflected by parallel-plate electrodes, the beam displacement D shown in Fig. 2(a) is given by the following equation:

$$D = \pm \frac{lb}{2a} \frac{V_d}{V_0}, \tag{1}$$

where a is the distance between the electrodes, b is the length of the electrodes, l is the working distance from the electrode center, and V_d is the deflection voltage. A deflection system consists of a waveform generator (Keysight Technologies, 33512B), a high-voltage and high-speed amplifier (Matsusada Precision, Inc., HOPS-3B1), and parallel-plate electrodes. Fig. 2(b) shows a simple schematic of a one-dimensional deflection system; however, the actual system has two pairs of electrodes, which can two-dimensionally deflect the ion beam. Voltage signals from the waveform generator are amplified

TABLE I. Specifications of ion beam gun.

Maximum accelerating voltage	5.0 kV
Maximum ion current	110 μA
Gaseous species	Argon
Type of plasma	ICP
Frequency of power supply	13.56 MHz
Base pressure	1.21×10^{-6} Pa

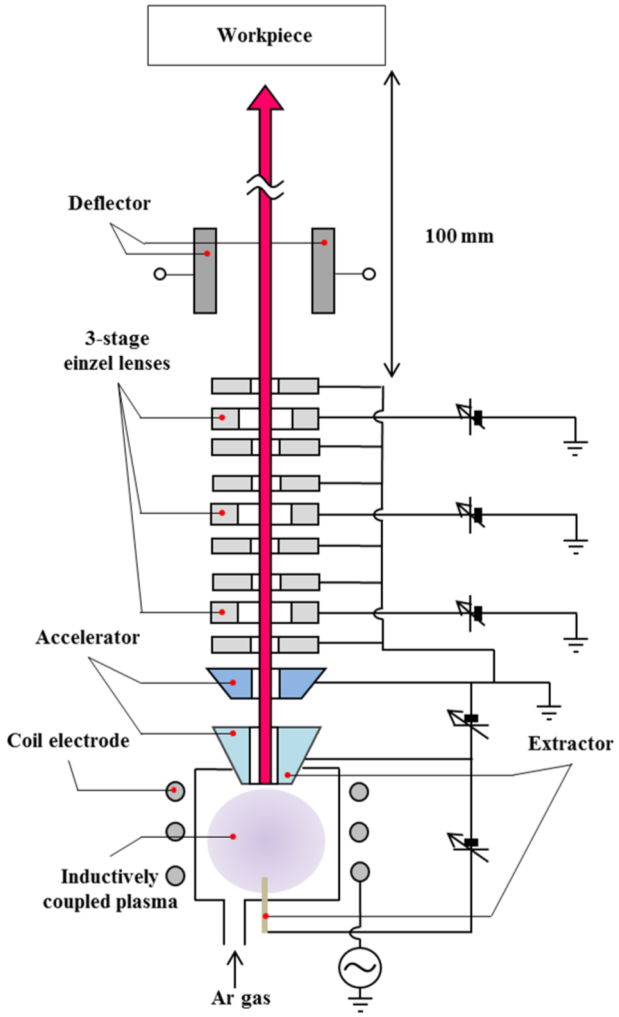

FIG. 1. Schematic of components of the ion beam gun.

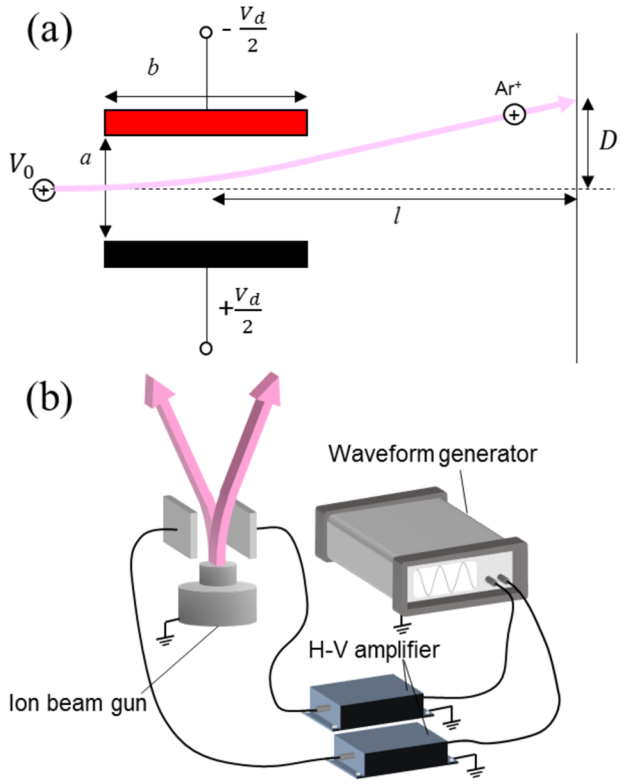

FIG. 2. Schematic of (a) principle of ion beam deflection and (b) developed deflection system.

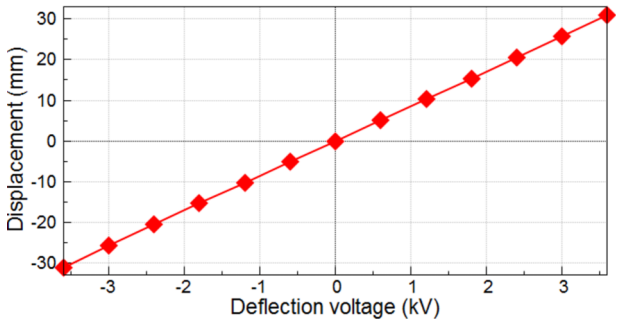

FIG. 3. Experimental relationship between the deflection voltage and the displacement of an ion beam at the sample plane.

by 300 times with the amplifier and generate an electric field in the path of the ion beam in the range of approximately $\pm 1.8 \times 10^5$ V/m, which corresponds to the deflection range of ±60 mm. By inputting arbitrary voltage signals to the waveform generator, we can deterministically scan the ion beam. To demonstrate the performance of the developed deflection system, we investigated the relationship between the deflection voltage and the displacement of an ion beam. We applied deflection voltages and obtained removal spots on a Cz-Si(001) ingot substrate. The displacement was obtained by measuring the shifts of the removal spots. As shown in Fig. 3, we could confirm that the displacement of an ion beam is precisely proportional to the deflection voltage. Deviations from the fitted linear function were approximately ~0.05 mm, which is in good agreement with the accuracy achieved when the shifts of the removal spots were measured.

III. EXPERIMENTS AND RESULTS

A. Evaluation of the stationary removal profile

We evaluated a stationary removal profile because it is an essential parameter for computer-controlled figuring. To obtain the shape of the stationary removal profile with an accuracy of ~1 nm, the following procedure was employed. A Cz-Si(001) ingot was masked and processed by a one-dimensionally deflected ion beam for 30 min, where the input voltage pattern signal to the deflection system for the sagittal direction was a triangle wave with peak-to-valley (PV) difference of 1.12 V and a frequency of 0.02 Hz. The detailed experimental conditions are shown in Table II. A processed surface and an unprocessed surface were obtained, as shown in Fig. 4(a). A one-dimensional stationary removal profile was precisely obtained by subtracting the cross-sectional shape along B-B′ from that along A-A′, as shown in Fig. 4(b), in which the profile along A-A′ represents the shape of the processed surface and that along B-B′ represents the shape of the unprocessed surface.

TABLE II. Experimental conditions for obtaining a stationary removal profile.

Work material	Cz-Si(001)
Accelerating voltage	5.0 kV
Einzel lens voltages	(4.0, 2.5, 3.8) kV
Ar flow rate	0.25 sccm
Applied RF power	55 W

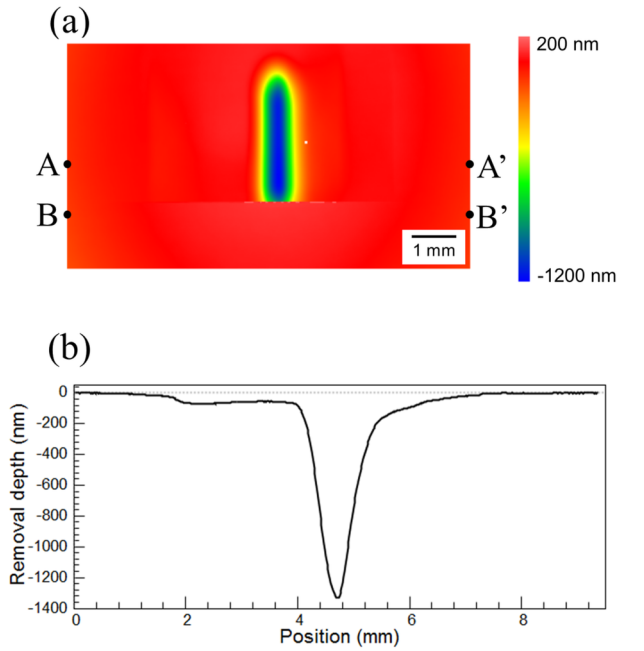

FIG. 4. (a) Measured shape of a stationary removal profile. (b) The one-dimensional stationary removal profile obtained by subtracting the cross sectional shape along B-B′ from that along A-A′.

B. Fabrication of the elliptical mirror and evaluation of the figuring accuracy

We fabricated a plano-elliptical mirror with an effective area of 30 mm × 3 mm to evaluate the figuring accuracy of the developed IBF system. This elliptical mirror was designed to have a focal length of 400 mm and a grazing-incidence angle of 3 mrad at the center of the mirror, which can focus X-rays at 10 keV down to 0.52 μm (FWHM). The target removal depth was calculated by subtracting a target elliptical shape from an initial shape, which ranged from 552 to 992 nm. In this experiment, shape profiles were measured by combining two stitching interferometers (MSI, RADSI), which were previously developed by our group and possess an accuracy less than 2 nm.[10,11] The distribution of dwelling time of an ion beam was determined by deconvolution of the target removal depth with the shape profile of the stationary removal spot. The

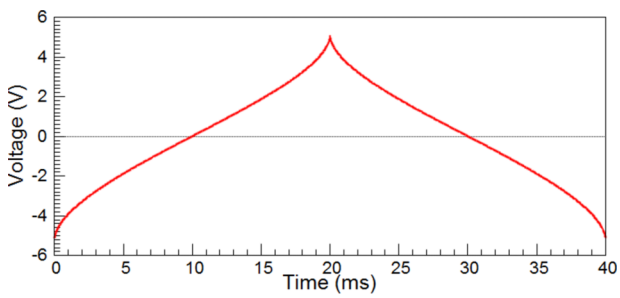

FIG. 5. Input voltage pattern to the waveform generator. This signal was output with a frequency of 25 Hz.

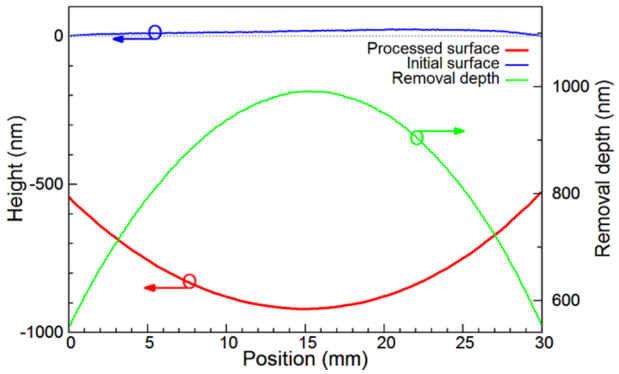

FIG. 6. Shapes of the mirror surface before (blue) and after (red) figuring, together with the actual removal depth (green), which was calculated by subtracting the processed shape from the preprocessed shape.

distribution of dwelling time was converted into the voltage pattern signal shown in Fig. 5. The elliptical shape was figured on a Cz-Si(001) ingot with dimensions of $50 \times 50 \times 10$ mm^3 (L × W × H). This substrate was nearly flat and was finished with non-disturbance polishing (Sharan Instruments Corporation). The sagittal shape profile of the substrate was perfectly flat at a local area over 1 mm in width, so that the ion beam was scanned with constant velocity in the sagittal direction. The input voltage pattern signal for the meridional direction is shown in Fig. 5, which was repeated with a frequency of 25 Hz. The signal for the sagittal direction was a triangle wave with a PV of 1.12 V and a frequency of 0.02 Hz. Experimental conditions were the same as those for obtaining the stationary removal spot. The processing time was 757.6 min.

Fig. 6 shows the measured shapes before and after processing and the actual removal depth. A nearly perfect elliptical shape was fabricated by figuring only once, and the residual figure errors from a fitted ellipse were about 4 nm PV, corresponding to 1.4 nm root mean square (RMS), as shown in Fig. 7 (solid line). The result indicated that the developed system possesses a figuring accuracy of 0.14% RMS, which was defined as RMS normalized by the maximum removal depth.

Next, additional figuring was carried out to correct the figure error. We obtained the shape profile of the stationary removal spot again by procedure described in Section III A. We calculated the voltage pattern signal from the residual figure errors. In the second figuring, experimental conditions were

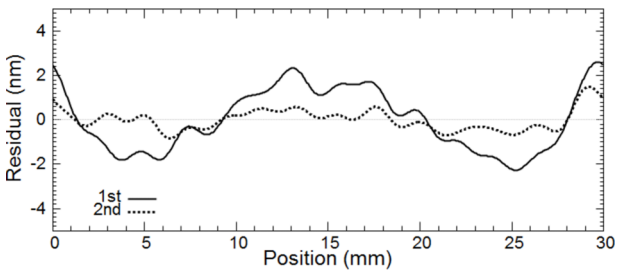

FIG. 7. Residual figure errors of the elliptical mirror. These data were processed using a low-pass filter with a cutoff spatial wavelength of 1.5 mm. After the 1st figuring, the residual figure error from a fit to an elliptical shape was only 4 nm PV and 1.4 nm RMS. After the 2nd figuring, the final residual error was approximately 1 nm PV and 0.48 nm RMS.

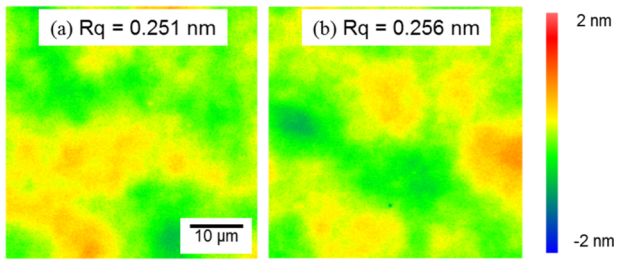

FIG. 8. Surface profiles (50×50 μm^2) of the (a) unprocessed surface and (b) processed surface, measured by white light interferometry.

the same as those in the first figuring. The processing time was 51.2 min. The dotted line in Fig. 7 shows the residual figure error after the second figuring. A residual figure error with approximately 1 nm PV, corresponding to 0.48 nm RMS, was achieved.

C. Investigation of surface roughness and ion beam smoothing (IBS)

The surface roughness was also investigated by white light interferometry (Zygo, NewView 5030) and atomic force microscopy (AFM) (Digital Instruments, Inc., Dimension 3100). First, the roughnesses of the processed surface and unprocessed surface were measured with white light interferometry. There was no change in the RMS roughness over a 50×50 μm^2 area, as shown in Fig. 8. Then, the higher-spatial-frequency surface roughness was measured with AFM. The roughness of the processed surface was 0.195 nm RMS over an area of 1×1 μm^2 (Fig. 9(b)). Compared to the unprocessed surface (Fig. 9(a)), the processed surface had a slightly higher RMS roughness because of irradiation by an ion beam with a 5-kV accelerating voltage. To improve the surface roughness, IBS[21] was carried out by using a low-energy ion beam produced by decreasing the accelerating voltage to 1 kV. The low-energy ion beam was irradiated onto the surface at an incident angle of 90°. In IBS, the ion beam was scanned along the sagittal direction, and the worktable under the mirror was moved at a constant velocity (0.5 mm/s) along the meridional direction to maintain the mirror shape. The processing time was about 3 h. The AFM image after IBS is shown in Fig. 9(c). The roughness was improved from 0.195 to 0.117 nm RMS. Power spectral density analysis indicated that microroughness with a spatial wavelength from 20 to 300 nm was successfully removed with IBS, as shown in Fig. 10. It is suggested that the fabricated mirror has a sufficiently smooth surface to ideally reflect X-rays.

IV. DISCUSSION

As shown in Fig. 7 (solid line), the residual figure error had a quartic shape. Possible causes are a slight disturbance of the electrical field or broadening of the ion beam depending on the displacement of the deflected beam. With respect to the former cause, the ion beam traveled in a slightly outer region from the center of the parallel-plate electrodes to separate neutral argons. In the outer region, the electrical field produced by

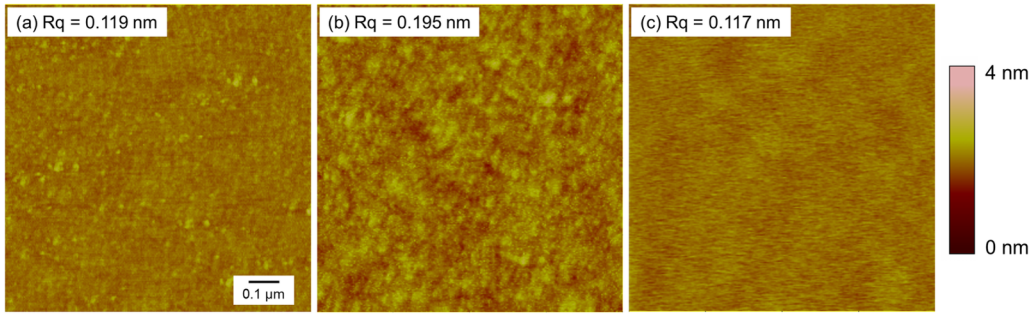

FIG. 9. Atomic force microscopy images of (a) the unprocessed surface, (b) the surface processed by a 5-kV ion beam, and (c) the surface smoothed by a 1-kV ion beam after figuring the elliptical shape.

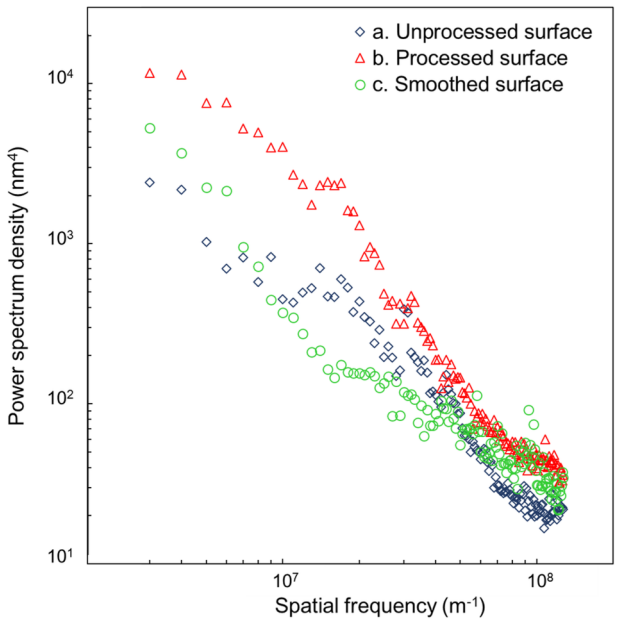

FIG. 10. Comparison of power spectral density functions of AFM images for various conditions.

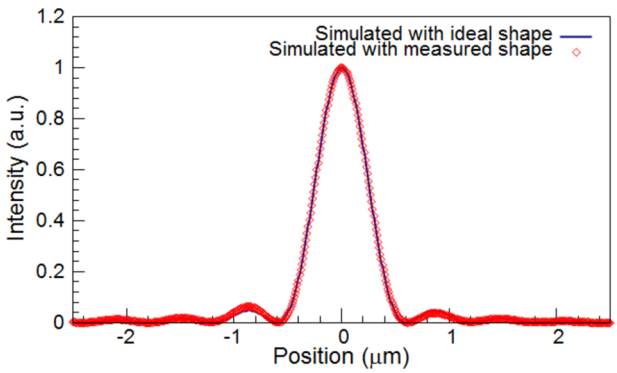

FIG. 11. One-dimensional beam profile at the focal plane simulated with an ideal shape (0.52 μm FWHM) and with the measured shape (0.53 μm FWHM).

the four electrodes was not exactly linear, which might have caused the systematic error. The latter cause suggests that the energy width of an ion beam is broadened by an electric field. The actual energy width was experimentally confirmed to be approximately 90 eV. However, this effect seems to be sufficiently small for a short mirror, because the expected broadening even at the end of the mirror is at most 0.05 mm. When fabricating longer mirrors, a noticeable influence will appear in the outermost region of the mirror. A new calculation algorithm for the dwelling time that is complementary to the beam broadening effect is under consideration.

To confirm that the fabricated mirror could focus X-rays, focused beam profiles were calculated using our wave-optical simulator[22] using the final shape. The X-ray energy used was 10 keV. The simulated result (Fig. 11) was in good agreement with the ideal focusing profile, which was calculated using an ideal elliptical mirror. These results indicated that the fabricated mirror can achieve almost fully diffraction-limited focusing.

V. SUMMARY AND OUTLOOK

An ion beam figuring system that utilizes electrostatic deflection was developed, and its figuring accuracy was investigated. The results indicated that the developed IBF system has a figuring accuracy of 0.14% RMS, which is significantly more accurate than that of the conventional figuring method using a mechanically scanning stage. An X-ray mirror with a shape accuracy of about 1 nm PV could be fabricated by figuring only twice. It is suggested that this non-contact and dry surface figuring method can be easily combined with X-ray metrology because the mirror substrate remained fixed during figuring. Additionally, the micro roughness was successfully reduced from 0.195 to 0.117 nm RMS by a low-energy ion beam.

We are improving the system to reach higher figuring accuracy by overcoming the previously mentioned systematic error. If an accuracy better than 0.1% is achieved, we may be able to finish X-ray mirrors that have a steeply curved shape without any dependence on metrology techniques. The achievable accuracy of current mirror fabrication, even with cutting edge techniques, is limited by optical metrology. Thus, if the processing itself is more precise, we will overcome this limitation. In the near future, next generation mirror fabrication methods will lead to more high-performance focusing optics.

ACKNOWLEDGMENTS

This research was partially supported by JSPS KAKENHI (Nos. 25600140, 23226004, and 26286077) from MEXT and the CREST project from JST. We would like to acknowledge Omegatron (Ibaraki, Japan) for assistance with the development of the ion beam gun.

[1]H. Mimura, S. Handa, T. Kimura, H. Yumoto, D. Yamakawa, H. Yokoyama, S. Matsuyama, K. Inagaki, K. Yamamura, Y. Sano, K. Tamasaku, Y. Nishino, M. Yabashi, T. Ishikawa, and K. Yamauchi, Nat. Phys. **6**, 122 (2009).
[2]M. Born and E. Wolf, *Principles of Optics*, 7th ed. (Cambridge University Press, Cambridge, 1999), pp. 527–532.
[3]K. Yamauchi, K. Yamamura, H. Mimura, Y. Sano, A. Saito, K. Endo, A. Souvorov, M. Yabashi, K. Tamasaku, T. Ishikawa, and Y. Mori, Appl. Opt. **44**, 6927 (2005).
[4]Y. Mori, K. Yamauchi, and K. Endo, Precis. Eng. **9**, 123 (1987).
[5]K. Yamauchi, H. Mimura, K. Inagaki, and Y. Mori, Rev. Sci. Instrum. **73**, 4028 (2002).
[6]Y. Mori, K. Yamamura, K. Yamauchi, K. Yoshii, T. Kataoka, K. Endo, K. Inagaki, and H. Kakiuchi, Nanotechnology **4**, 225 (1993).
[7]K. Yamamura, K. Yamauchi, H. Mimura, Y. Sano, A. Saito, K. Endo, A. Souvorov, M. Yabashi, K. Tamasaku, T. Ishikawa, and Y. Mori, Rev. Sci. Instrum. **74**, 4549 (2003).
[8]A. Shorey, W. Kordonski, and M. Tricard, Proc. SPIE **5533**, 99–107 (2004).
[9]M. Ando, M. Negishi, M. Takimoto, A. Deguchi, and N. Nakamura, Nanotechnology **6**, 111 (1995).
[10]K. Yamauchi, K. Yamamura, H. Mimura, Y. Sano, A. Saito, K. Ueno, K. Endo, A. Souvorov, M. Yabashi, K. Tamasaku, T. Ishikawa, and Y. Mori, Rev. Sci. Instrum. **74**, 2894 (2003).
[11]H. Mimura, H. Yumoto, S. Matsuyama, K. Yamamura, Y. Sano, K. Ueno, K. Endo, Y. Mori, M. Yabashi, K. Tamasaku, Y. Nishino, T. Ishikawa, and K. Yamauchi, Rev. Sci. Instrum. **76**, 045102 (2005).
[12]F. Siewert, T. Noll, T. Schlegel, T. Zeschke, and H. Lammert, AIP Conf. Proc. **705**, 847 (2007).
[13]S. G. Alcock, K. J. S. Sawhney, S. Scott, U. Pedersen, R. Walton, F. Siewert, T. Zeschke, F. Senf, T. Noll, and H. Lammert, Nucl. Instrum. Methods Phys. Res., Sect. A **616**, 224 (2010).
[14]S. G. Alcock, L. Nistea, J. P. Sutter, K. Sawhney, J.-J. Fermé, C. Thellier, and L. Peverini, J. Synchrotron Radiat. **22**, 10 (2015).
[15]Y. Takeda, Y. Hata, K. Endo, and K. Yamamura, J. Phys. D: Appl. Phys. **47**, 115503 (2014).
[16]H. Yumoto, H. Mimura, S. Matsuyama, S. Handa, Y. Sano, M. Yabashi, Y. Nishino, K. Tamasaku, T. Ishikawa, and K. Yamauchi, Rev. Sci. Instrum. **77**, 063712 (2006).
[17]A. Schindler, T. Hänsel, D. Flamm, W. Frank, G. Böhm, F. Frost, R. Fechner, F. Bigl, and B. Rauschenbach, Proc. SPIE **4440**, 217–227 (2001).
[18]T. Arnold, G. Böhm, R. Fechner, J. Meister, A. Nickel, F. Frost, T. Hänsel, and A. Schindler, Nucl. Instrum. Methods Phys. Res., Sect. A **616**, 147–156 (2010).
[19]E. Ziegler, L. Peverini, I. V. Kozhevnikov, T. Weitkamp, and C. David, AIP Conf. Proc. **879**, 778 (2007).
[20]S. Matsuyama, H. Yokoyama, R. Fukui, Y. Kohmura, K. Tamasaku, M. Yabashi, W. Yashiro, A. Momose, T. Ishikawa, and K. Yamauchi, Opt. Express **20**, 24977 (2012).
[21]F. Frost, R. Fechner, B. Ziberi, D. Flamm, and A. Schindler, Thin Solid Films **459**, 100 (2004).
[22]S. Matsuyama, H. Mimura, H. Yumoto, K. Yamamura, Y. Sano, K. Endo, Y. Mori, Y. Nishino, K. Tamasaku, T. Ishikawa, M. Yabashi, and K. Yamauchi, Rev. Sci. Instrum. **76**, 083114 (2005).